Hindawi
International Journal of Antennas and Propagation
Volume 2022, Article ID 4136347, 13 pages
https://doi.org/10.1155/2022/4136347

Research Article

Aperture-Fed Quad-Port Dual-Band Dielectric Resonator-MIMO Antenna for Sub-6 GHz 5G and WLAN Application

Trushit Upadhyaya,[1] **Ikmo Park**,[2] **Rajat Pandey**,[1] **Upesh Patel**,[1] **Killol Pandya**,[1] **Arpan Desai**,[1] **Jayesh Pabari**,[3] **Gangil Byun**,[4] **and Yogeshwar Kosta**[1]

[1]*Electronics and Communication Department, Chandubhai S. Patel Institute of Technology, Charotar University of Science and Technology, Changa, Gujarat, India*
[2]*Department of Electrical and Computer Engineering, Ajou University, Republic of Korea*
[3]*Physical Research Laboratory, Ahmedabad, Gujarat, India*
[4]*Ulsan National Institute of Science and Technology (UNIST), Ulsan, Republic of Korea*

Correspondence should be addressed to Trushit Upadhyaya; trushitupadhyaya.ec@charusat.ac.in

Received 10 March 2022; Revised 10 May 2022; Accepted 8 July 2022; Published 28 August 2022

Academic Editor: Flaminio Ferrara

A four-port dielectric resonator-based connected ground multiple-input multiple-output (MIMO) antenna is designed. The presented antenna was excited through the aperture feeding technique. The dual bands are achieved by optimally feeding the rectangular dielectric resonator through engineered triangular slots. The antenna has operating modes of TE^{X}_{111} and TE^{Y}_{111} at 4.5 GHz and 5 GHz, respectively. It presents a 2 : 1 VSWR bandwidth of 2.64% (4.48 GHz–4.60 GHz) and 1.2% (4.96 GHz–5.04 GHz) in the lower and upper bands, respectively. The edge-to-edge distance between array elements is around 7.5 mm. The single antenna dimension is 30 mm × 30 mm, whereas the four-port antenna dimension is 60 mm × 60 mm. The optimum isolation was achieved by carefully placing the antenna elements on the substrate through multiple iterations. The antenna provides port isolation better than 20 dB at both resonances with full ground profile. The advantage of the antenna is that it provides fair antenna and MIMO parameters without additional isolation techniques. The antenna has efficiency in order of 88.02% and 86.31%. The peak gain is 7.67 dBi and 8.32 dBi at 4.5 GHz and 5 GHz, respectively. The optimum envelope correlation coefficient (ECC) is 0.037, channel capacity coss (CCL) is 0.2 bits/sec/Hz, diversity gain (DG) is 9.99 dB, and total active reflection coefficient (TARC) is −18.87. The antenna elements are orthogonally placed with adequate separation to achieve polarization diversity and spatial diversity. The antenna provides the utilization in Sub-6 GHz 5G and WLAN communication applications.

1. Introduction

The need for faster communication is rapidly increasing with the rising demand for multimedia and real-time traffic data. Co-channel interference is one of the key issues while accommodating users within the same spectrum. High-speed streaming needs advanced technological requirements beyond the 3G and 4G communication systems. The 5G communication technology provides quite a high data rate without any major sacrifice in the user bandwidth [1, 2]. The 5G system has much lower latency and delay compared to the earlier communication systems. With the evolution of each generation, a multifold rise in data rate has been attained by employing advanced technology. The multiple-input multiple-output (MIMO) technology facilitates the requirements of a 5G communication system, and it is expected to also provide the platform for the 6G communication system. In 5G communication, it was necessary to cover multiple frequency resonances to provide coverage to a range of standards and also provide diverse gains within the allocated bands. The MIMO technology provides high spectrum efficiency to facilitate seamless connectivity. The 5 G communication system supports a significantly higher count of mobile users with unobtrusive connectivity through adequate frequency channel allocation.

To improve communication reliability, the 5G technology employs multiple antennas. The MIMO technology addresses the multipath fading issue by sending data from multiple transmitting antennas to multiple receiving antennas. The information received by each antenna is different as it undergoes inconsistent fading across different antennas. A wide range of multiplexing schemes is in existence for providing degrees of freedom by the use of MIMO technology. The mobile terminals are posing a space-constrained environment. Planar and surface-mountable antennas are the most viable choices for supporting multiple antenna systems [1, 2]. The planar, typically patch, antennas also offer suitability in the manufacturing process and cost-effectiveness. The patch antenna suffers from constraints of limited bandwidth and gains while fabricated on substrates posing high dielectric losses. On the other hand, dielectric resonator antennas (DRAs) give higher radiation efficiency while adequate excitation is employed. The adequate implementation of geometric attributes leads to lower conduction losses, resulting in higher efficiency. There is a compact list of literature on the utilization of dielectric resonators for the design of MIMO antennas compared to traditional antennas [3–10]. It becomes possible to optimize the antenna parameters such as front-to-back ratio, beamwidth, bandwidth, and cross-polarization by appropriately designing the dielectric material. The multiple resonant modes can be excited by the appropriate selection of size and shape of the dielectric resonator. The presented dielectric resonator-MIMO could excite modes of TE^{X}_{111} and TE^{Y}_{111} to achieve dual-band resonance.

One of the prime factors affecting the isolation between the ports of the MIMO antenna is the spacing between the elements on the antenna. There has been significant research available in the literature for improvement in the port isolation across the antenna element, especially by introducing isolating elements or networks [11–20]. There is substantial research on multiband MIMO wireless communication [21–27]. It is extremely challenging to achieve antenna compactness and high levels of port isolation simultaneously. The port isolation can be attained by an adequate organization of resonators on the feeding elements in the nonexistence of the decoupling mechanism. The internal decoupling of the modes is frequently employed for attaining port isolation. The optimized dimensions of the resonators will ensure different current directions to avoid strong interelement coupling. There shall be a constraint in dimension optimization for the large number of the resonators, causing coupling between the elements, which makes port isolation poor for the antenna. It becomes vital to address the challenge of compromise between port isolation and antenna electrical size. The present communication technology requires an antenna with multiple resonant frequencies. This requirement also applies to the MIMO antennas. The dielectric resonator excited by the patch antenna is one of the techniques adopted for MIMO communication. The engineered patch antennas can excite the dielectric resonator through aperture coupling of fields.

2. Antenna Configuration

The engineered MIMO dielectric resonator antenna is depicted in Figure 1. The top and perspective views of the antenna have been exhibited for distinction. Initially, only the rectangular-shaped patch resonator fed by the microstrip line is designed. The key feature of the dielectric resonator is the absence of metal, where the conducting loss tends to be large at high frequencies. The traditional conductor-based antenna suffers considerably from such metallic losses. The radiation efficiency of such antennas is quite good, which provides high antenna gain. If an adequate dielectric constant is selected, then these antennas tend to provide larger bandwidth than traditional patch antennas. An alumina material with a dielectric constant of 9.9 having a loss tangent of 0.0001 has been utilized for the antenna design because of its cost-effectiveness and wide availability. Figure 2 illustrates the design evolution. The dielectric resonator was fed through a slit on the patch by means of aperture feeding. The position of the slot was chosen by doing the parametric study and observing its effects on the reflection coefficient of the proposed aperture-fed DRA MIMO. It was observed that the coupling varies as we vary the position of the slot, and hence an optimized value providing better coupling was chosen. The shapes and dimensions of the slots on the patch were altered to excite the resonating modes. The excitation of fundamental TE^{X}_{111} mode along with TE^{Y}_{111} mode is the signature feature for achieving desired antenna resonance characteristics. Table 1 tabulates the physical dimensions of the proposed antenna.

The dielectric material is excited through the aperture coupling technique, through the electromagnetic coupling of a field being emitted from a conducting patch. Microstrip feed excitation is used for conducting patches. The microstrip feed technique provides the least design complexity while exciting the patch antenna. The excited patch further induces the field, which gets coupled with the DR. The DR gets excited through aperture coupling. The standard FR-4 substrate is employed in the dielectric resonator (DR) antenna design. The typical 70 μm copper sheets were considered on top of the FR4 dielectric resonator for simulation. The dielectric resonator has an equal length and width of 16 mm and a height of 10 mm. A full-wave finite element-based numerical software is used for the implementation of the proposed DR-MIMO antenna. The core reason for employing the square DR compared to circular and/or cylindrical resonators is the feasibility and degree of freedom for the optimization process in the antenna design. The secondary reason is to avoid degenerated modes being produced. It is quite difficult to derive a prediction model for antenna resonance, while the combination of resonator and patch is utilized. It is only possible through numerous simulations to achieve the target resonances. However, close prediction can be taken up by using the DRA excitation mode equations.

The engineered dimensions of rectangular dielectric resonators were numerically computed using the following equations to generate the fundamental TE_{111} mode to meet the target resonance. The numerically computed resonance

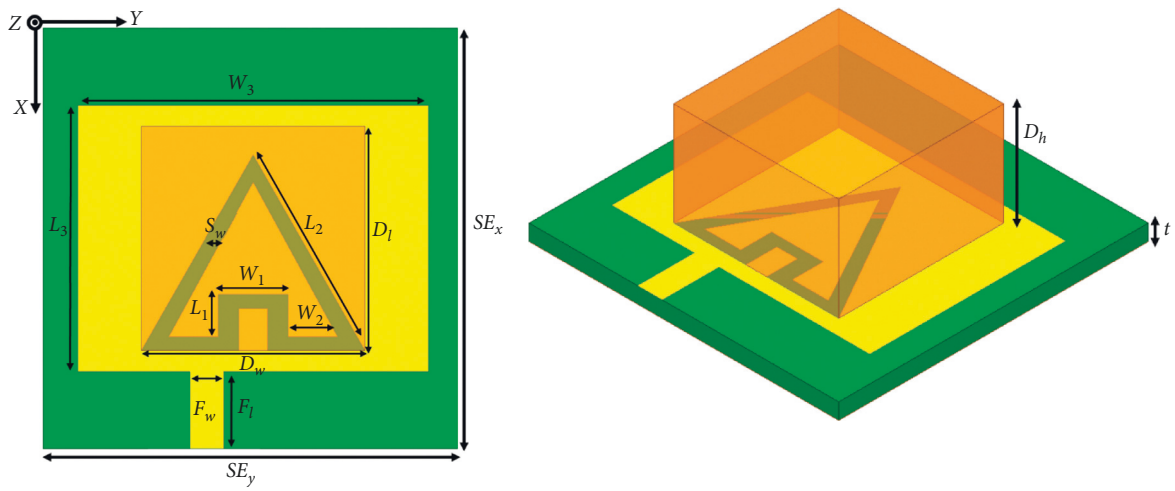

(a) (b)

Figure 1: The proposed antenna element view: (a) top and (b) perspective.

of the resonator is 4.53 GHz whereas the simulated resonances of the fundamental TE^X_{111} and TE^Y_{111} are achieved at 4.5 GHz and 5 GHz. It can be seen that the numerically computed and simulated values are fairly close. Through the simulations, fundamental modes can be observed using electric field simulation within the dielectric resonator as shown in Figure 3. The dissimilarity in these resonances is due to the fact that the dielectric waveguide model does not consider the adopted feeding technique [8].

Through the simulations, higher-order modes can be observed using electric field simulations within the dielectric resonator. The E-field distribution in the x-z and y-z cross-section of the dielectric resonator at 4.5 GHz and 5 GHz has been displayed in Figures 3(a) and 3(b), respectively. It can be validated that TE^X_{111} and TE^Y_{111} modes are excited. The computation of the resonant modes of the rectangular DRA can be taken up by using the following equations as per the dielectric waveguide model [8]:

$$k_z \tan\left(\frac{k_z d}{2}\right) = \sqrt{(\varepsilon_r - 1)\left(k_z^2\right) - k_z^2},$$

$$k_x^2 + k_y^2 + k_z^2 = \varepsilon_r k_o^2,$$

$$k_x = \frac{m\pi}{a}, \quad (1)$$

$$k_y = \frac{n\pi}{b},$$

$$k_o = \frac{2\pi}{\lambda_o},$$

where k_o is the free-space wavenumber; k_x, k_y, and k_z are half-wave variations; a, b, and d are the length, width, and height of the resonating element.

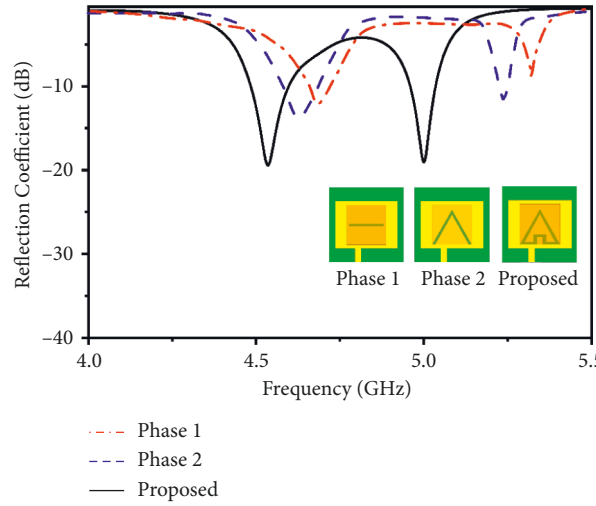

Figure 2: Design evolution.

3. Parametric Optimization in Antenna Design

Apparently, there are multiple physical parameters of the antenna which can affect the radiation fields. Intuitively, these alterations will affect the antenna radiation parameters such as resonance, directivity, polarization, bandwidth, and beamwidth, to name a few.

Multiple iterations were carried out to obtain the target resonance from the proposed antenna. Out of many possible iterated combinations, a few of the parametric variations are exhibited in Figure 4. The variation in resonator length and width is shown in Figures 4(a) and 4(b). The variations in height of the dielectric resonator are exhibited in Figure 4(c). The DR height was varied to see the optimum response around the targeted resonance. The selection of the DR height is crucial as the antenna volume will increase significantly with an increase in

Table 1: Physical dimensions of proposed single element antenna.

Parameter	Dimensions (mm)	Parameter	Dimensions (mm)	Parameter	Dimensions (mm)
$\mathbf{SE_x}$	30	D_h	10	W_1	5
L_1	3	D_w	16	W_2	3.5
L_2	16	D_l	16	$S_x = S_y$	60
L_3	19	F_w	2.4	SE_y	30
t	1.56	F_l	5.5	S_w	1

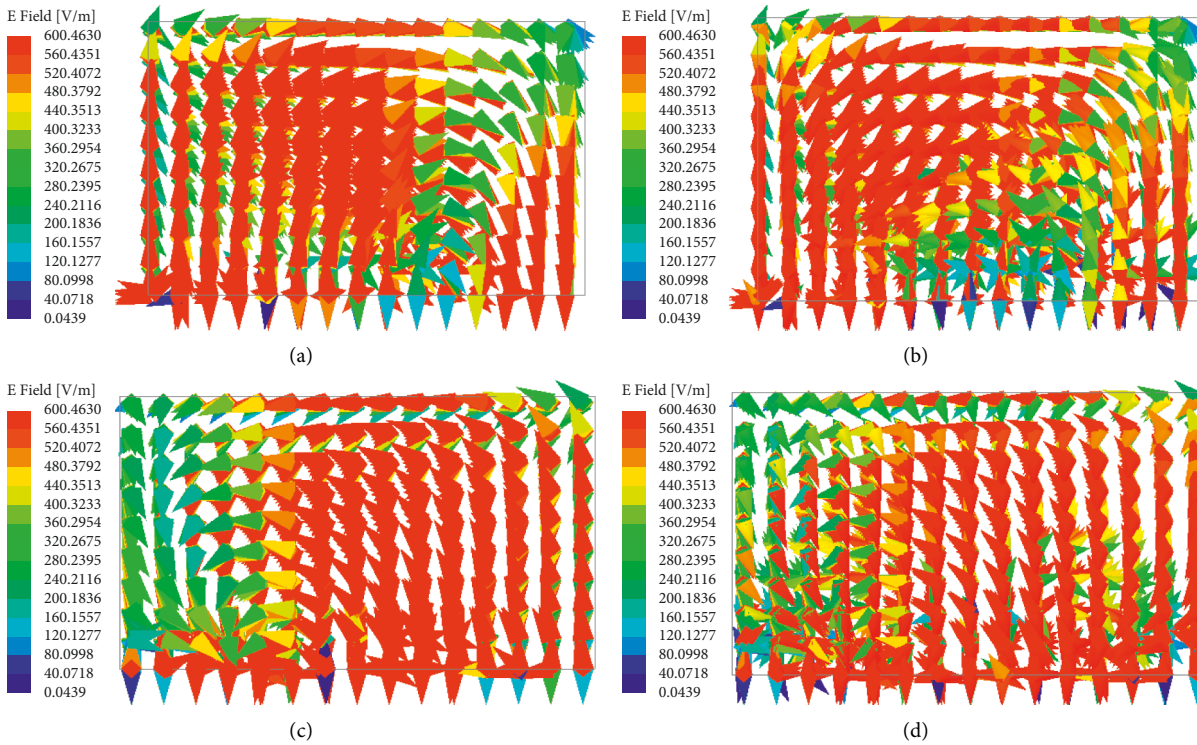

Figure 3: Excited E-field. (a) 4.5 GHz (x-z), (b) 5 GHz (x-z), (c) 4.5 GHz (y-z), and (d) 5 GHz (y-z).

DR height. Increased DR height may improve the antenna parameters; however, antenna placement or mounting must be considered by the design engineer. All displayed dimensions are in mm. It is extremely challenging to have an empirical relationship between changes in an antenna's physical dimensions and the antenna resonance. By modifying the height of DRA, it was observed that antenna resonance was reduced. This is well expected as by altering the height of DRA, the effective dielectric constant of the antenna will vary. Similar variations were carried out for changes in the DRA length and width. The field coupling will vary with the change in the slot beneath the DRA. Hence, the antenna resonance will vary. The triangular slots were initially tried for analyzing the antenna resonance. To further tune it further near to the targeted resonance, inner arms were taken up. The impact of variation of arm slots has been depicted in Figure 4(d). This was also demonstrated in the antenna evolution. All the dimensions were varied in multiple iterations to optimize the antenna for the target frequencies.

4. MIMO Antenna Configuration

The MIMO antenna configuration is exhibited in Figure 5. The proposed MIMO antenna has four elements. It is intuitive that to minimize the interelement mutual coupling and provide adequate spatial diversity, the substrate dimensions were increased adequately while maintaining the full ground profile. Multiple iterations were carried out to optimize the antenna's electrical compactness without compromising the port isolation. Similarly, an orthogonal arrangement of the patch with dielectric resonators was performed to achieve polarization diversity. The substrate length (S_X) and width (S_Y) are kept at 60 mm each, and the optimized MIMO antenna dimensions are $60 \times 60 \times 1.56\,\text{mm}^3$. The MIMO antenna model is exhibited in Figure 5. The DRs are attached to the patch elements with the use of a thin layer of conducting adhesive.

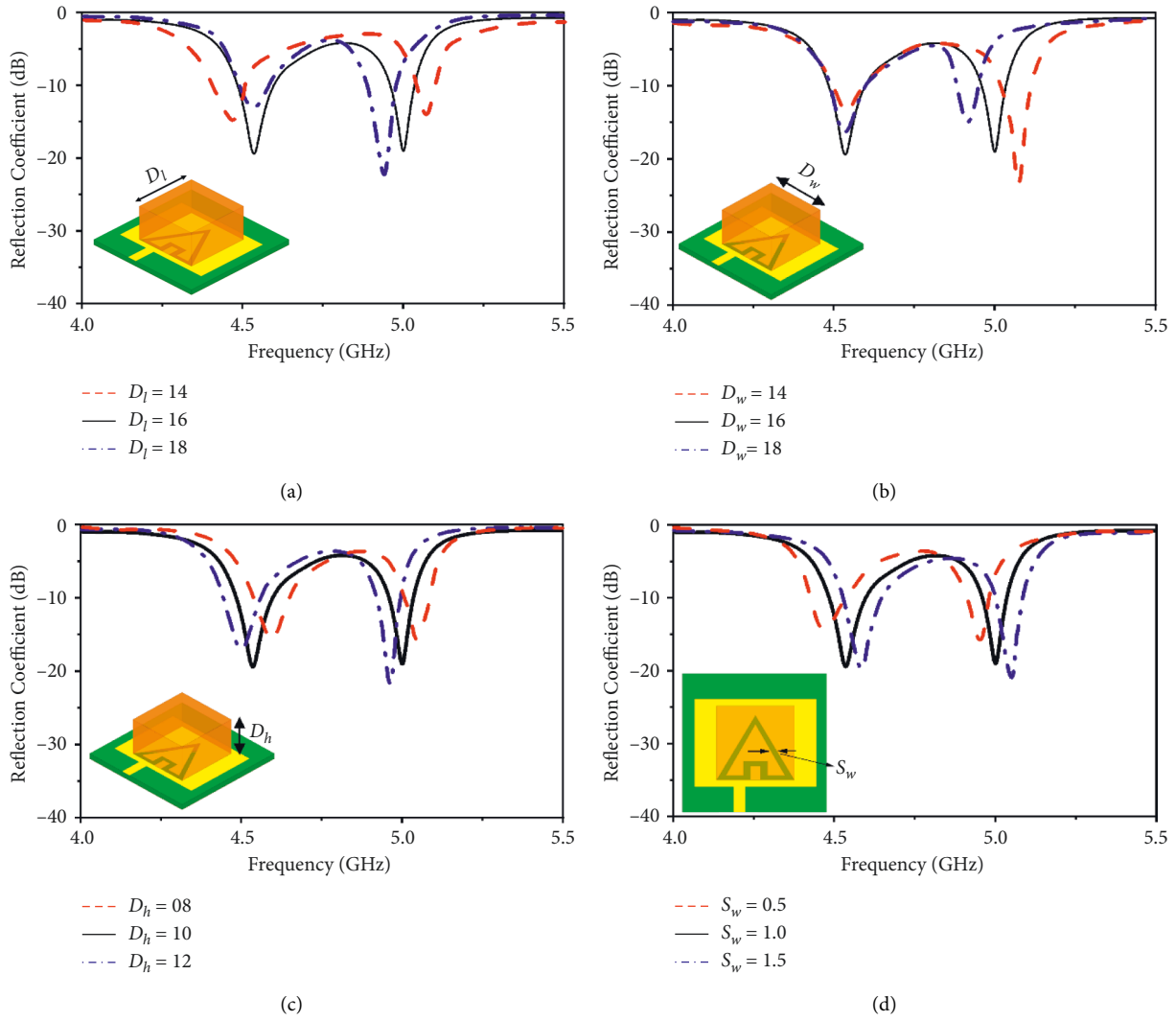

Figure 4: Parametric study of DRA. (a) length, (b) width, (c) height, (d) slot width.

5. Results and Discussions

The measurement of antenna parameters was carried out on the fabricated antenna prototype as depicted in Figure 6. The alumina material was prepared by using laser cutting technology. Keysight benchtop Vector Network Analyzer E5063A was utilized for reflection coefficient measurements. The dual-band antenna resonates at 4.5 GHz and 5 GHz. The simulated resonances are illustrated in Figure 7(a), and measured resonances are illustrated in Figure 7(b).

There appears to be a fair correlation between these results. The reflection coefficient is measured at a port by keeping the remaining ports terminated at 50 Ω. The achieved fractional bandwidth for VSWR is better than 2 : 1, in the order of 2.64% (4.48 GHz–4.60 GHz) and 1.2% (4.98 GHz–5.04 GHz) has been achieved. The frequencies cover the sub-6 GHz and WLAN communication targets. The S_{11} is only depicted due to the identical nature of S_{11} and S_{22}. A port isolation of 22.5 dB and 24.98 dB has been attained for 4.5 GHz and 5 GHz, respectively. It is expected to have port isolation above 20 dB for good diversity performance.

The chosen topology for the proposed quad element DRA MIMO antenna was selected in order to achieve the necessary isolation levels, which should be greater than 15 dB. The antenna elements are arranged in an orthogonal fashion to reduce the mutual coupling amongst the elements and thus achieve the anticipated MIMO diversity performance. Various other topologies, such as mirror symmetric alignment along vertical and horizontal directions, were also simulated in the simulator. All the topologies provided satisfactory results. The reason for choosing the orthogonal topology is that it provides polarization diversity, which has the advantage of providing better isolation performance while keeping the structure compact. However, the other topologies provide spatial diversity wherein to achieve the desired isolation performance, and the antenna footprint increases.

It is noteworthy that in the proposed antenna, no isolation mechanism was employed to attain port isolation of such magnitude. Figures 8 and 9 represent the antenna radiation pattern and gain/efficiency against frequency. The cross-pol isolations for both frequencies are satisfactory. The omnidirectional radiation pattern was achieved at both

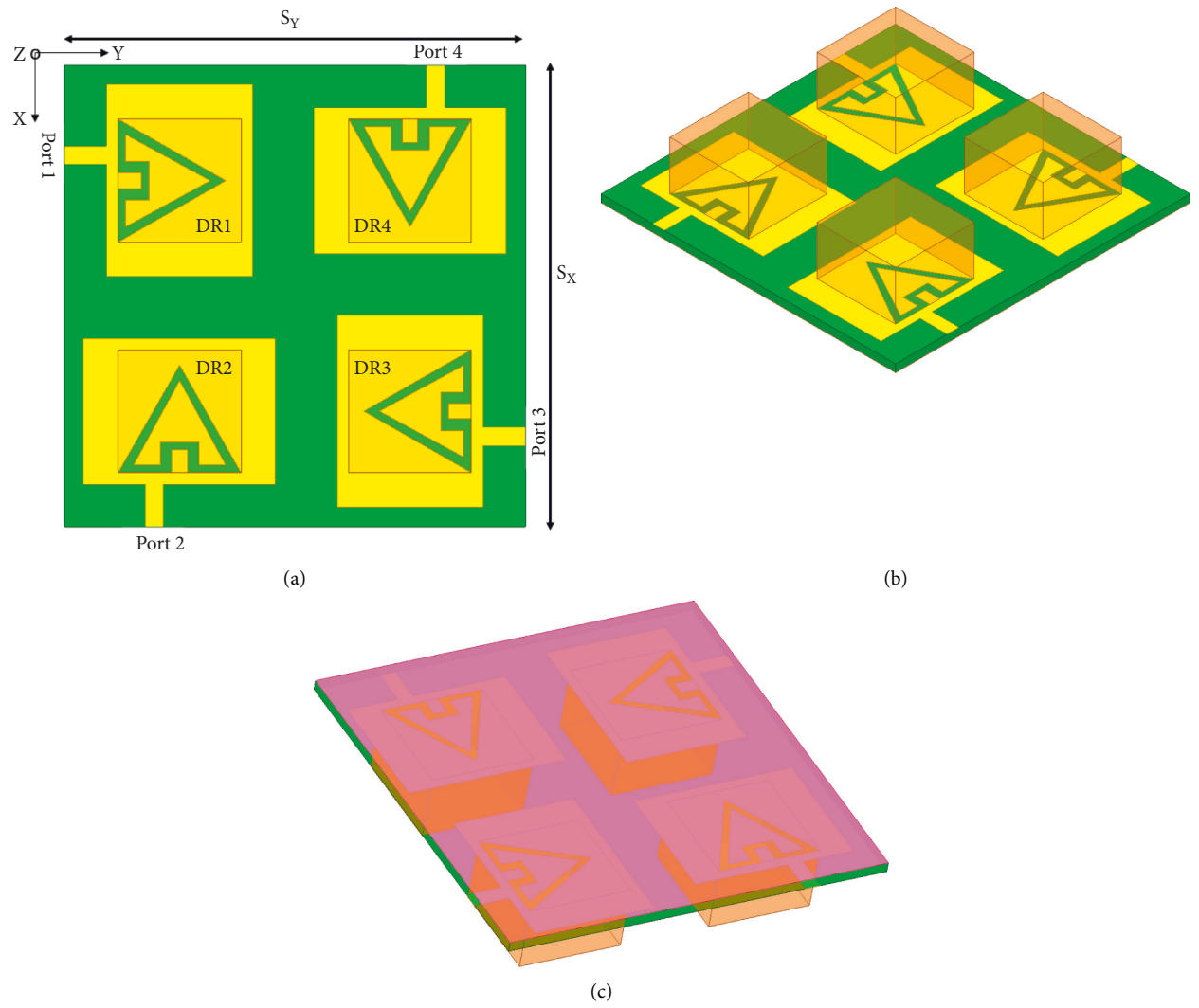

Figure 5: Proposed MIMO antenna: (a) top view, (b) top perspective view, and (c) bottom perspective view (full ground profile).

frequencies. The antenna has an efficiency of 88.02% and 86.31%. The peak gain is 7.67 dBi and 8.32 dBi at 4.5 GHz and 5 GHz, respectively.

6. MIMO Diversity Performance

The primary reason to employ the MIMO antenna is to provide diversity. The diversity techniques improve the reliability of the communication by employing high spectrum efficiency and a faster data rate. The MIMO diversity techniques aid in the effective utilization of the channel capacity despite the presence of fading environment. The performance parameters were analyzed to examine the antenna diversity performance, namely, the envelope correlation coefficient (ECC), the channel capacity loss (CCL), mean effective gain (MEG), and total active reflection coefficient (TARC). The ECC performance shows the correlation between the antenna radiation patterns. If two patterns are inhomogeneous, then they shall not correlate, for instance, a vertically polarized pattern shall not correlate with the horizontally polarized pattern. The correlation shall be zero for the case if the direction of radiation is opposite from the radiating elements. For the multiple antenna systems, the ECC amongst i^{th} and j^{th} resonator can be analyzed using the far-field patterns as given in the following equation:

$$\rho e = \mathrm{ECC} = \left| \frac{\iint_0^{4\pi} [\overrightarrow{\mathbf{F1}}(\theta, \varnothing) * \overrightarrow{\mathbf{F2}}(\theta, \varnothing)] d\Omega |2}{\iint_0^{4\pi} |\overrightarrow{\mathbf{F1}}(\theta, \varnothing)| 2 d\Omega \iint_0^{4\pi} |\overrightarrow{\mathbf{F2}}(\theta, \varnothing)| 2 d\Omega} \right|. \tag{2}$$

$R_i(\theta, \phi)$ and $R_j(\theta, \phi)$ are 3D-pattern when i^{th} and j^{th} port are excited, ω is the solid angle, $*$ is the Hermitian product, and θ and ϕ are elevation and azimuth angles, respectively. It is anticipated that ECC should be less than 0.5; for the designed antenna, the ECC values are around 0.037 and 0.002 as illustrated in Figure 10. These are well within the acceptable levels of ECC.

The antenna diversity gain (DG) provides an improvement in signal-to-noise ratio (SNR) when the MIMO antenna diversity scheme is established. With the existence of the MIMO system, the SNR is enhanced, and subsequently the signal reception. This improves the reliability of the

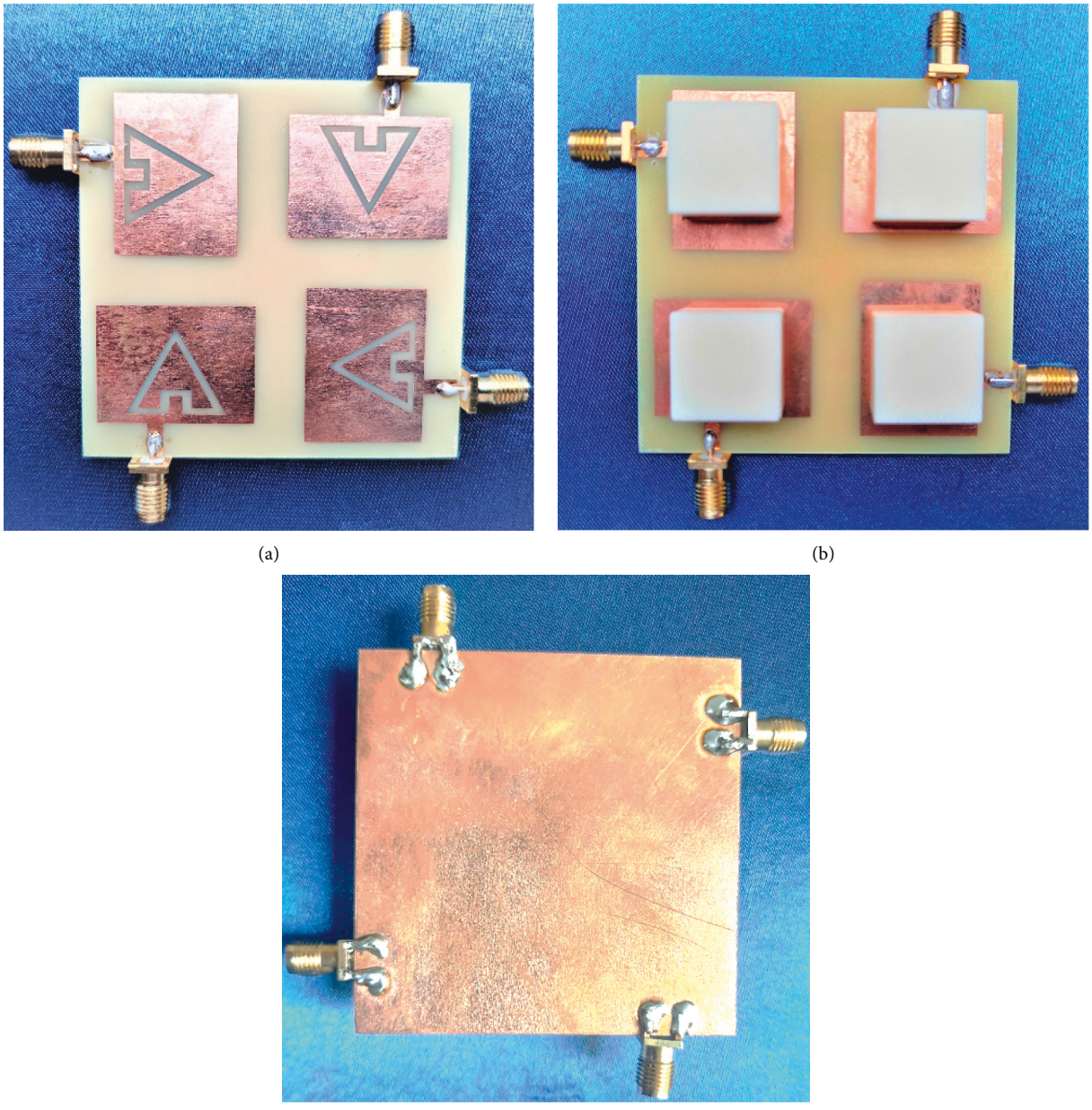

(a) (b) (c)

Figure 6: Proposed MIMO antenna: (a) top view without DR, (b) top view with DR, and (c) bottom view.

communication system. The DG can be computed from calculated values of ECC as shown in (3). The values are depicted in Figure 11. The calculated values along with other diversity parameters are tabulated in Table 2.

$$\mathrm{DG} = 10\sqrt{1 - |0.99\,\mathrm{ECC}|^2}. \tag{3}$$

The MEG provides the received power for the MIMO antenna in comparison to the isotropic antenna. The calculation of the presented antenna is shown in (4). The presented antenna has four-port hence i will take up value up to four. Owing to the lower coupling between the antenna elements, the MEG of the proposed antenna is good. MEG values are depicted in Figure 12 for corresponding resonances.

$$\mathrm{MEG}_i = 0.5\left[1 - \sum_{j=1}^{N} \left|S_{ij}\right|^2\right]. \tag{4}$$

The TARC provides the ratio of reflected to incident power for the n-port MIMO antenna. The S and N represent the scattering matrix and count of MIMO antenna elements, respectively. The value of TARC is less than −18.87 dB, as shown in Figure 13. This exhibits a very low reflection coefficient of the overall antenna system and less coupling between the elements. The inter-element isolation is a key diversity component of MIMO antenna design. Typically, the channel capacity increases substantially with an increase in the resonating elements in the MIMO antenna. However, the tight coupling and footprint tradeoff become vital for the

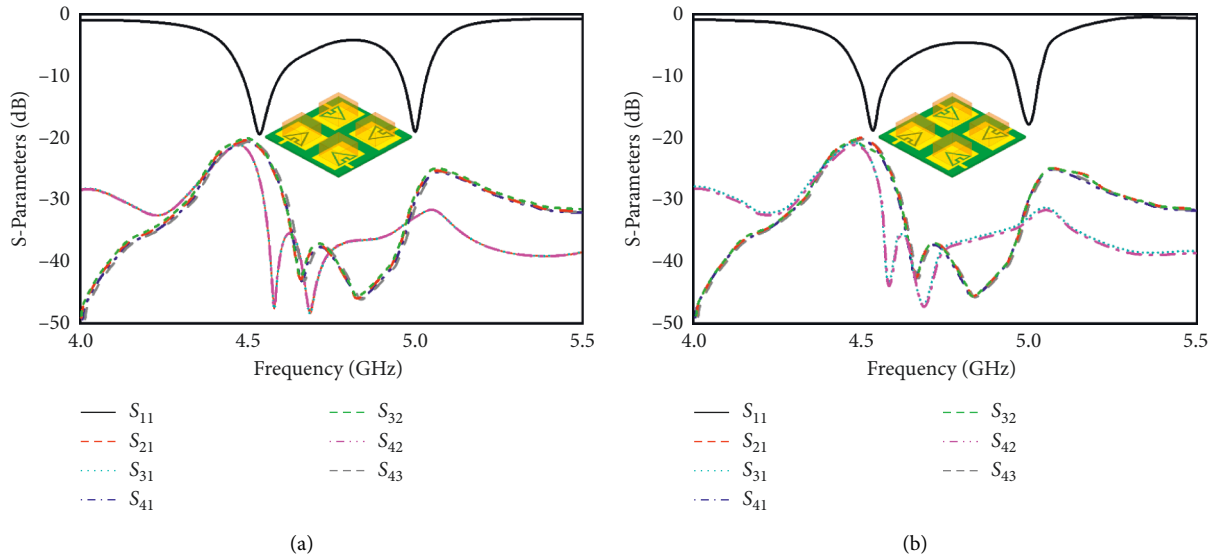

Figure 7: Scattering parameters (a) simulated and (b) measured.

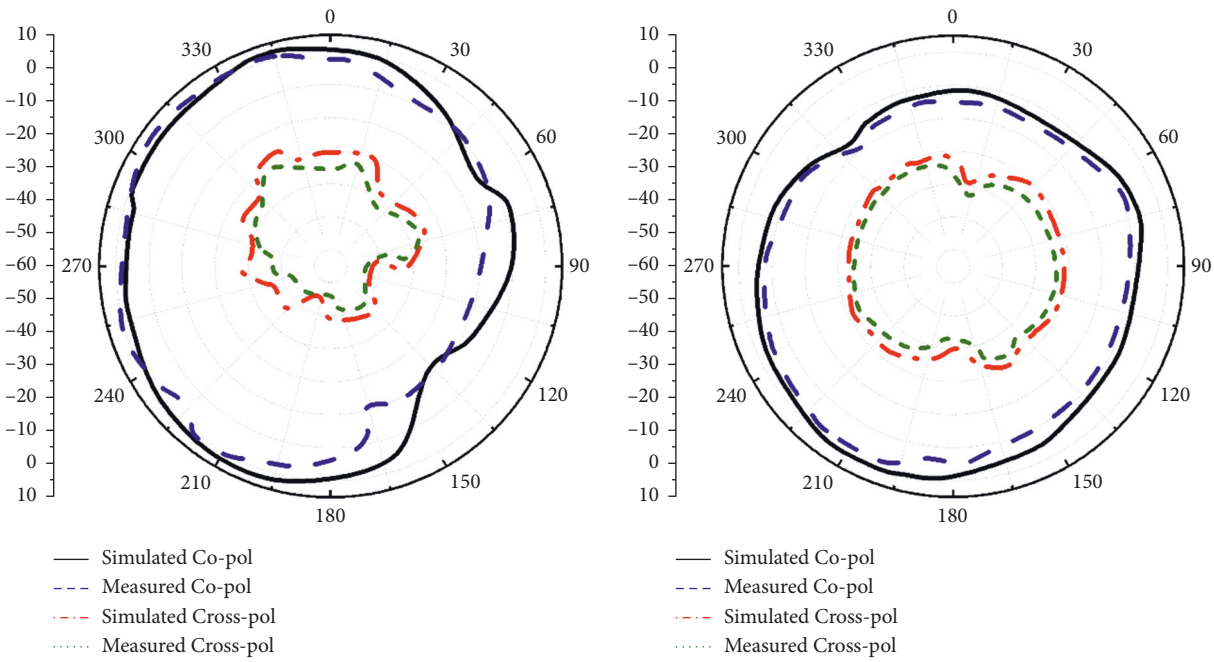

Figure 8: Continued.

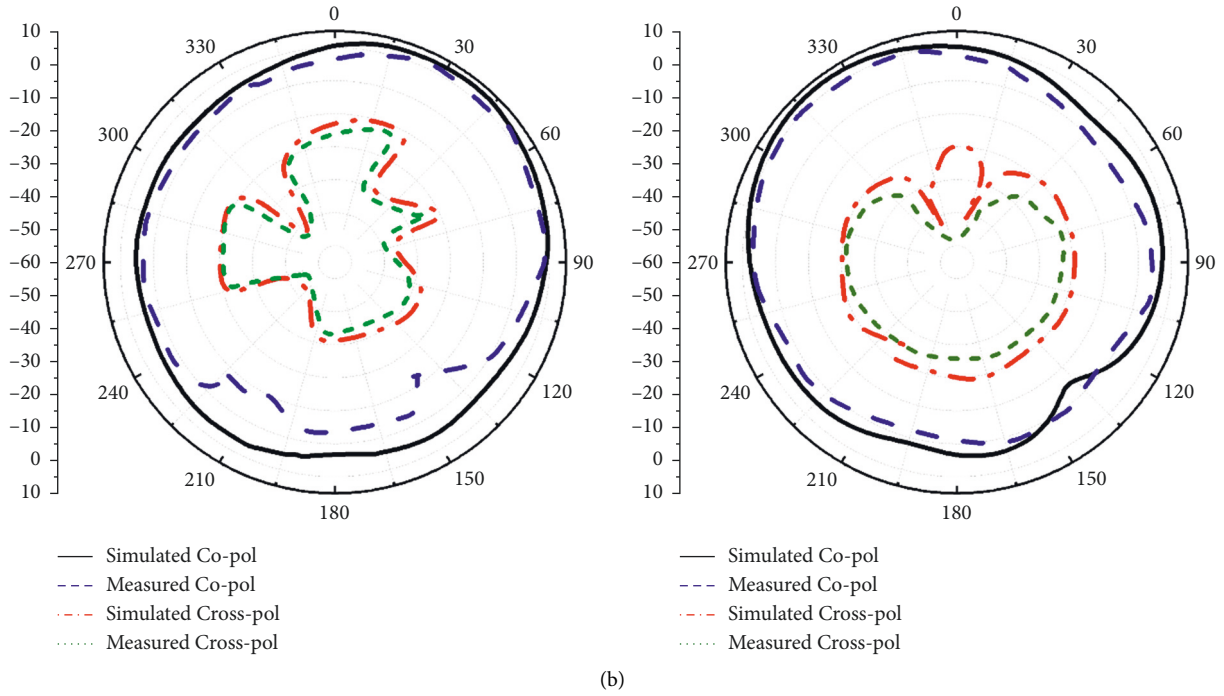

(b)

Figure 8: Antenna radiation pattern (a) 4.5 GHz and (b) 5 GHz.

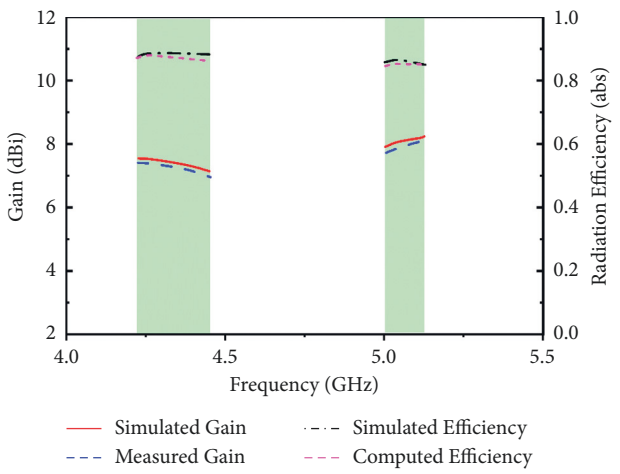

Figure 9: Variation of gain and efficiency with frequency.

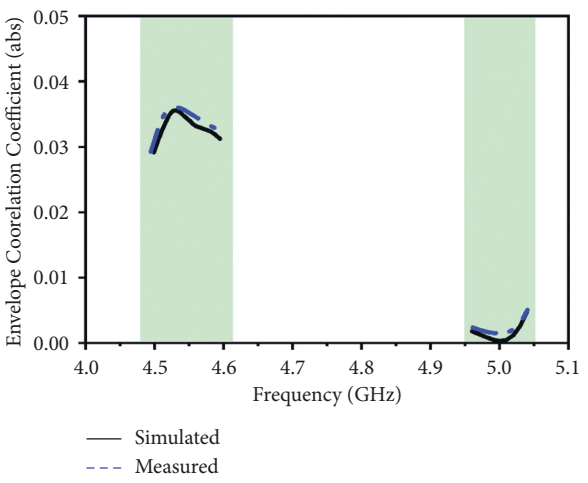

Figure 10: Simulated and measured ECC.

design as the increase in element count will considerably increase the coupling between the elements. The CCL was computed by Eq. (7) and it has been exhibited in Figure 14. The suitable value of the CCL is 0.6 bits/sec/Hz and the proposed MIMO antenna is within the permissible range. Table 3 tabulates the comparison of the proposed antenna with published literature, and it is apparent that the proposed antenna is well suited for the targeted communication applications. The antenna exhibits quite improved characteristics in terms of electrical size and gain.

$$\mathrm{TARC} = \frac{\sqrt{\sum_{n=1}^{N} |b_n|^2}}{\sqrt{\sum_{n=1}^{N} |a_n|^2}}, \tag{5}$$

$$b_n = [S]a_n, \tag{6}$$

$$\mathrm{CCL} = -\log_2 \det\left(\Psi^R\right), \tag{7}$$

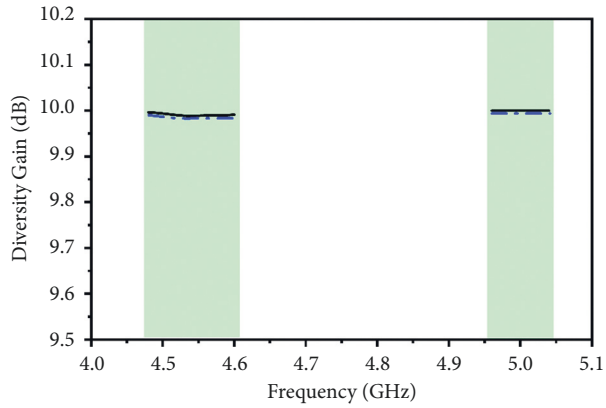

Figure 11: Simulated and measured DG.

Table 2: Antenna diversity parameters.

Frequency (GHz)	ECC	DG (dB)	MEG (dB)	TARC (dB)	CCL(bits/sec/Hz)
4.5	0.037	9.9999	1.0005	−24.91	0.2
5.0	0.002	9.9999	1.0002	−18.87	0.78

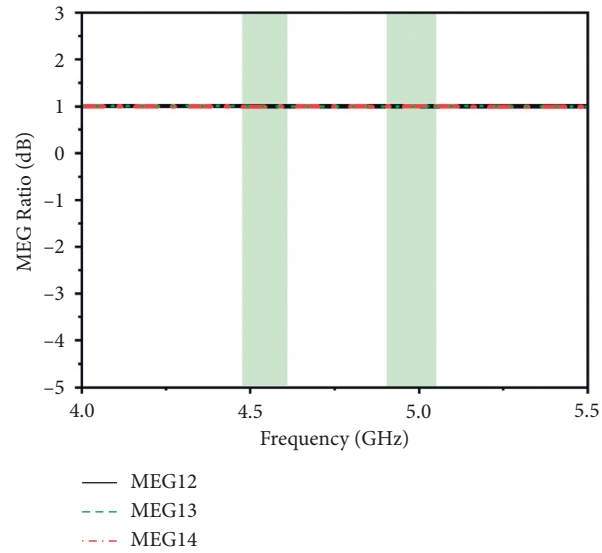

Figure 12: Mean effective gain of MIMO antenna.

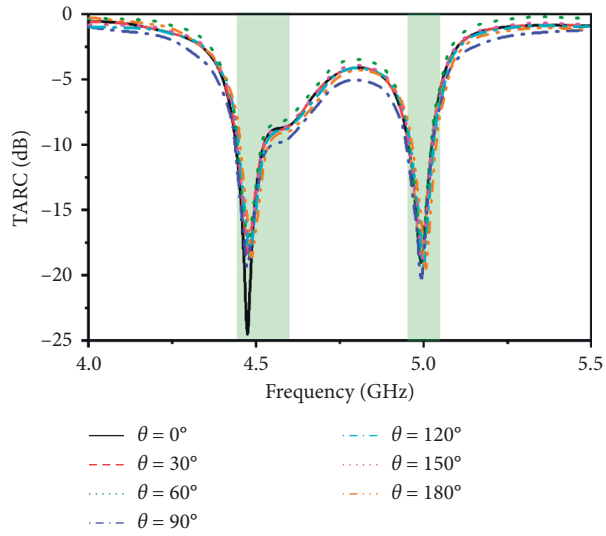

Figure 13: Proposed MIMO antenna TARC.

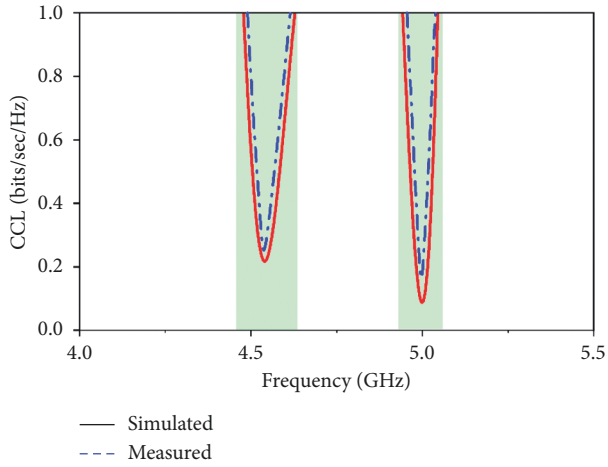

Figure 14: Proposed MIMO antenna CCL.

Table 3: Comparison of the proposed antenna with literature.

Citation	Operating frequencies (GHz)	Antenna size (λ)	Gain (dBi)	Bandwidth (%)	Efficiency (%)	Feed type	Design complexity
[28]	4.9	2.28 × 0.73 x 0.13	6.2	5.1	—	Microstrip line	Low
[29]	3.22–3.97, 4.95–5.51	0.86 × 0.86 x 0.12	5.2 5.5	4.97, 2.35	95	Microstrip line	Low
[30]	5.71–8.2, 7.57–7.95	1.53 × 1.53 x 0.12	−1.9, 3.8	34.85, 4.55	—	Microstrip line	Low
[31]	3.40–4.13	1.13 × 1.13 x 0.19	8.1	19.4	>90	Probe feed	High
[32]	3.50–5.10	1.43 × 1.43 x 0.36	8.5	45	88	Probe feed	High
[33]	4.56–9.96	1.5 × 1.5 x 0.39	—	74	—	Trapezoidal patch	Medium
[34]	4.33–7.02	2.6 × 2.6 x 0.36	—	47.4	89	Probe	High
Proposed antenna	4.5, 5	0.89 × 0.89 x 0.17	7.67, 8.32	2.64%, 1.2%	88.02, 86.31	Aperture couple	Medium

$$\Psi^R = \begin{bmatrix} \rho_{11}\,\rho_{12}\,\rho_{13}\,\rho_{14} \\ \rho_{21}\,\rho_{22}\,\rho_{23}\,\rho_{24} \\ \rho_{31}\,\rho_{32}\,\rho_{33}\,\rho_{34} \\ \rho_{41}\,\rho_{42}\,\rho_{43}\,\rho_{44} \end{bmatrix}, \tag{8}$$

$$\begin{aligned} \rho_{ii} &= 1 - \sum_{n=1}^{4} \left(S_{in}^{*} S_{ni}\right), \\ \rho_{ij} &= -\sum_{n=1}^{4} \left(S_{in}^{*} S_{nj}\right), \quad \text{For} i, j = 1, 2, 3 \text{or} 4. \end{aligned} \tag{9}$$

7. Conclusion

An aperture coupled DRA antenna is presented. Electromagnetic coupling in feeding characterizes the dual-band operation of the antenna by suitably optimizing the physical properties of the antenna. The excitation of fundamental TE_{111}^{X} and TE_{111}^{X} mode is utilized to achieve the desired antenna resonance characteristics. The antenna provides the bandwidth in the order of 2.64% and 1.2% along with the gain of 7.67 dBi and 8.32 dBi at 4.5 GHz and 5 GHz, respectively. The optimum envelope correlation coefficient (ECC) is 0.037, channel capacity loss (CCL) is 0.2 bits/sec/Hz, diversity gain (DG) is 9.99 dB, and total active reflection coefficient (TARC) is −18.87. The diversity performance of the proposed antenna meets the necessary requirements of 5G and WLAN communication applications.

Data Availability

None.

Conflicts of Interest

The authors declare that they have no conflicts of interest.

References

[1] M. S. Sharawi, "Printed multi-band MIMO antenna systems and their performance metrics [wireless corner]," *IEEE Antennas and Propagation Magazine*, vol. 55, no. 5, pp. 218–232, 2013.

[2] M. P. Karaboikis, V. C. Papamichael, G. F. Tsachtsiris, C. F. Soras, and V. T. Makios, "Integrating compact printed antennas onto small diversity/MIMO terminals," *IEEE Transactions on Antennas and Propagation*, vol. 56, no. 7, pp. 2067–2078, 2008.

[3] H. Huang, X. Li, and Y. Liu, "A low-profile, dual-polarized patch antenna for 5G MIMO application," *IEEE Transactions on Antennas and Propagation*, vol. 67, no. 2, pp. 1275–1279, 2019.

[4] Y. Li, Z. Zhao, Z. Tang, and Y. Yin, "Differentially fed, dual-band dual-polarized filtering antenna with high selectivity for 5G sub-6 GHz base station applications," *IEEE Transactions on Antennas and Propagation*, vol. 68, no. 4, pp. 3231–3236, 2020.

[5] C. H. Le Thi, S. X. Ta, X. Q. Nguyen, K. K. Nguyen, and C. Dao-Ngoc, "Design of compact broadband dual-polarized antenna for 5G applications," *International Journal of RF and Microwave Computer-Aided Engineering*, vol. 31, no. 5, Article ID e22615, 2021.

[6] S. Chouhan, D. K. Panda, V. S. Kushwah, and P. K. Mishra, "Octagonal-shaped wideband MIMO antenna for human interface device and S-band application," *International Journal of Microwave and Wireless Technologies*, vol. 11, no. 3, pp. 287–296, 2019.

[7] S. K. Yadav, A. Kaur, and R. Khanna, "Compact rack shaped MIMO dielectric resonator antenna with improved axial ratio for UWB applications," *Wireless Personal Communications*, vol. 117, no. 2, pp. 591–606, 2021.

[8] P. Rajat Girjashankar and T. Upadhyaya, "Substrate integrated waveguide fed dual band quad-elements rectangular dielectric resonator MIMO antenna for millimeter wave 5G wireless communication systems," *AEU-international Journal of Electronics and Communications*, vol. 137, Article ID 153821, 2021.

[9] S. U. Anuar, M. H. Jamaluddin, J. Din, K. Kamardin, M. H. Dahri, and I. H. Idris, "Triple band MIMO dielectric resonator antenna for LTE applications," *AEU-international Journal of Electronics and Communications*, vol. 118, Article ID 153172, 2020.

[10] A. K. Dwivedi, A. Sharma, A. K. Singh, and V. Singh, "Circularly Polarized Quad-Port MIMO Dielectric Resonator Antenna with Beam Tilting Feature for Vehicular Communication," *IETE Technical Review*, pp. 1–13, 2020.

[11] M. Alibakhshikenari, F. Babaeian, B. S. Virdee et al., "A comprehensive survey on "various decoupling mechanisms with focus on metamaterial and metasurface principles applicable to SAR and MIMO antenna systems"," *IEEE Access*, vol. 8, pp. 192965–193004, 2020.

[12] Z. Wang, C. Li, Q. Wu, and Y. Yin, "A metasurface-based low-profile array decoupling technology to enhance isolation in MIMO antenna systems," *IEEE Access*, vol. 8, pp. 125565–125575, 2020.

[13] A. Bhattacharjee, A. Karmakar, A. Saha, and D. Bhattacharya, "Design of a compact UWB MIMO-diversity antenna incorporating fractal inspired isolation structure with band notch characteristics," *Microwave and Optical Technology Letters*, vol. 63, no. 10, pp. 2597–2605, 2021.

[14] Z. Yang, J. Xiao, and Q. Ye, "Enhancing MIMO antenna isolation characteristic by manipulating the propagation of surface wave," *IEEE Access*, vol. 8, pp. 115572–115581, 2020.

[15] J. Tang, F. Faraz, X. Chen et al., "A metasurface superstrate for mutual coupling reduction of large antenna arrays," *IEEE Access*, vol. 8, pp. 126859–126867, 2020.

[16] J. Y. Deng, J. Y. Li, and L. X. Guo, "Decoupling of a three-port MIMO antenna with different impedances using reactively loaded dummy elements," *IEEE Antennas and Wireless Propagation Letters*, vol. 17, no. 3, pp. 430–433, 2018.

[17] S. Roy and U. Chakraborty, "Mutual coupling reduction in a multi-band MIMO antenna using meta-inspired decoupling network," *Wireless Personal Communications*, vol. 114, no. 4, pp. 3231–3246, 2020.

[18] K. H. Moussa, A. S. I. Amar, M. Mabrouk, and H. G. Mohamed, "Slotted E-shaped meta-material decoupling slab for densely packed MIMO antenna arrays," *Micromachines*, vol. 12, no. 8, p. 873, 2021.

[19] M. Li and S. Cheung, "A novel calculation-based parasitic decoupling technique for increasing isolation in multiple-element MIMO antenna arrays," *IEEE Transactions on Vehicular Technology*, vol. 70, no. 1, pp. 446–458, 2021.

[20] C. F. Ding, X. Y. Zhang, C. D. Xue, and C. Y. D. Sim, "Novel pattern-diversity-based decoupling method and its

application to multielement MIMO antenna," *IEEE Transactions on Antennas and Propagation*, vol. 66, no. 10, pp. 4976–4985, 2018.

[21] S. Kumar, D. Nandan, K. Srivastava et al., "Wideband circularly polarized textile MIMO antenna for wearable applications," *IEEE Access*, vol. 9, pp. 108601–108613, 2021.

[22] J. Huang, G. Dong, J. Cai, H. Li, and G. Liu, "A quad-port dual-band MIMO antenna array for 5G smartphone applications," *Electronics*, vol. 10, no. 5, p. 542, 2021.

[23] A. Pant, M. Singh, and M. S. Parihar, "A frequency reconfigurable/switchable MIMO antenna for LTE and early 5G applications," *AEU-international Journal of Electronics and Communications*, vol. 131, Article ID 153638, 2021.

[24] D. El Hadri, A. Zakriti, A. Zugari, M. El Ouahabi, and J. El Aoufi, "High isolation and ideal correlation using spatial diversity in a compact MIMO antenna for fifth-generation applications," *International Journal of Antennas and Propagation*, vol. 2020, Article ID 2740920, pp. 1–10, 2020.

[25] X. Jin, Y. Qiu, D. Wu et al., "A low-profile dual-polarized MIMO antenna with an AMC surface for WLAN applications," *International Journal of Antennas and Propagation*, vol. 2021, Article ID 9218255, pp. 1–12, 2021.

[26] P. Laxman and A. Jain, "Circularly polarized wideband fabric stealth multiple-input multiple-output antenna for ultra-wideband Applications useful for wireless systems wearable on garments," *International Journal of Antennas and Propagation*, vol. 2021, Article ID 1426680, pp. 1–16, 2021.

[27] M. Daghari, C. Essid, and H. Sakli, "Muli-UWB Antenna System Design for 5G Wireless Applications with Diversity," *Wireless Communications and Mobile Computing*, vol. 2021, Article ID 9966581, 2021.

[28] G. Ali Sarkar, S. Ballav, A. Chatterjee, S. Ranjit, and S. K. Parui, "Four element MIMO DRA with high isolation for WLAN applications," *Progress In Electromagnetics Research Letters*, vol. 84, pp. 99–106, 2019.

[29] A. K. Dwivedi, A. Sharma, A. K. Singh, and V. Singh, "Design of dual band four port circularly polarized MIMO DRA for WLAN/WiMAX applications," *Journal of Electromagnetic Waves and Applications*, vol. 34, no. 15, pp. 1990–2009, 2020.

[30] G. Varshney, R. Singh, V. S. Pandey, and R. S. Yaduvanshi, "Circularly polarized two-port MIMO dielectric resonator antenna," *Progress In Electromagnetics Research M*, vol. 91, pp. 19–28, 2020.

[31] S. Fakhte and H. Oraizi, "Compact uniaxial anisotropic dielectric resonator antenna operating at higher order radiating mode," *Electronics Letters*, vol. 52, no. 19, pp. 1579-1580, 2016.

[32] B. Mukherjee, P. Patel, and J. Mukherjee, "Hemispherical dielectric resonator antenna based on apollonian gasket of circles—a fractal approach," *IEEE Transactions on Antennas and Propagation*, vol. 62, no. 1, pp. 40–47, 2014.

[33] A. Sharma and A. Biswas, "Wideband multiple-input–multiple-output dielectric resonator antenna," *IET Microwaves, Antennas & Propagation*, vol. 11, no. 4, pp. 496–502, 2017.

[34] S. Maity and B. Gupta, "Experimental investigations on wideband triangular dielectric resonator antenna," *IEEE Transactions on Antennas and Propagation*, vol. 64, no. 12, pp. 5483–5486, 2016.